

Thickness of a European Ice Shell from Impact Crater Simulations

E. P. Turtle* and E. Pierazzo

Several impact craters on Jupiter's satellite Europa exhibit central peaks. On the terrestrial planets, central peaks consist of fractured but competent rock uplifted during cratering. Therefore, the observation of central peaks on Europa indicates that an ice layer must be sufficiently thick that the impact events did not completely penetrate it. We conducted numerical simulations of vapor and melt production during cratering of water ice layers overlying liquid water to estimate the thickness of Europa's icy crust. Because impacts disrupt material well beyond the zone of partial melting, our simulations put a lower limit on ice thickness at the locations and times of impact. We conclude that the ice must be more than 3 to 4 kilometers thick.

Evidence for a liquid water layer beneath Europa's icy surface includes thermal analyses (1-4), Voyager and Galileo observations of geologic features (5-11), and Galileo observations of an induced magnetic dipole field (12, 13). Galileo gravity measurements constrain the total thickness of Europa's outer layer of ice and liquid water to 80 to 170 km (14), but they cannot distinguish different phases. The thickness of an ice shell has important implications for the shell's tectonics and internal dynamics, such as whether solid-state convection is possible (15, 16). However, the thickness of the ice is controversial, with estimates ranging from only 1 to 2 kilometers (11, 17-19) to at least a few tens of kilometers (20-22). Here, we report on the results of numerical simulations of vapor and melt production during crater formation in layers of ice overlying liquid water and their

implications for the thickness of Europa's ice shell.

Impact crater morphology depends not only on the impact energy, but also on the gravity, the material properties, and the near-surface structure of the target. Despite their small number, European impact structures are widely distributed (Fig. 1). They span a broad range of diameters and they demonstrate a suite of crater morphologies that appears to be correlated with crater size (23). Primary craters <~5 km in diameter have the bowl shape typical of simple craters. Most larger structures resemble complex craters found elsewhere in the solar system and several exhibit central peaks (Fig. 2). The two largest impact structures on Europa [Web fig. 1 (24)] consist of central disrupted regions >50 km in diameter surrounded by several concentric fractures with diameters ≤100 km. The craters exhibit subdued topographic expression; stereo observations limit depths to ≤500 m (23, 25).

Observations of several terrestrial complex craters (26), as well as Copernicus on the Moon (27), have demonstrated that central peaks consist of deeply buried material that is uplifted

during crater formation. Although the material is fractured, it moves coherently, preserving stratigraphic relations (28). Therefore, the depths to which European central peak craters penetrate during the early stages of cratering provide lower limits on the thickness of an ice shell at the times and locations of crater formation.

We conducted simulations of impacts into an ice shell overlying liquid water (Table 1) with the two-dimensional, finite-difference, Eulerian-Lagrangian hydrocode called CSQ (29) coupled to the ANEOS (analytical equation of state) package (30). The spatial resolution of the Eulerian mesh was kept to 30 to 40 cells per projectile radius in each simulation. One hundred Lagrangian tracer particles were regularly distributed in the target to record its thermodynamic history at intervals of 5 ms. From the shock pressures recorded, we determined the regions in which the target material is completely vaporized and completely melted (Table 1 and Fig. 3).

More than 90% of the craters on the Galilean satellites are caused by the impact of Jupiter-family comets (31). The distribution of the cumulative impact velocity (31) implies a median impact velocity for Jupiter-family comets on Europa of ~26.5 km/s. Therefore, we primarily modeled comets that impact the surface vertically at 26.5 km/s. We also ran simulations with projectile velocities of 21.5 and 30.5 km/s to investigate the effect on melting and vaporization. For numerical convenience, we assumed comet compositions of 100% water ice.

Material porosity affects the partitioning of impact energy between target and impactor; a porous projectile requires more energy to close the pores, therefore decreasing the amount of energy partitioned to the target. Because comets' porosities are unknown, we used two values for the projectile density, a lower limit of 0.6 g/cm³ (32) and an upper limit of 1.1 g/cm³, corresponding to the full density (no porosity) of the ANEOS for water ice [Web table (24)].

Lunar and Planetary Laboratory, University of Arizona, Tucson, AZ 85721, USA.

*To whom correspondence should be addressed. E-mail: turtle@lpl.arizona.edu

Table 1. Model parameters and results of hydrocode simulations. Proj., projectile; diam., diameter; trans., transient; temp., temperature; vol., volume; CV, complete vaporization; CM, complete melting; max., maximum; melt., melting; cond., conductive; conv., convective; PC, purely conductive ice over liquid water; CL, conductive lid over convecting ice.

Figure	Proj. diam. (km)	Proj. density (g/cm ³)	Impact velocity (km/s)	Trans. crater diam. (km)	Ice thickness (km)	Temp. profile	CV vol. (km ³)	CM vol. (km ³)	Max. CV depth (km)	Max. CM depth (km)	Max. depth of 50% melt. (km)
3F	0.50	1.1	26.5	12.3	3.0*	CL	0.365	6.035	0.91	2.12	4.37
3C	1.00	1.1	26.5	21.2	3.0*	CL	3.162	119.33	1.85	6.85	8.59
	0.50	1.1	26.5	12.3	4.0	PC	0.369	5.544	0.91	1.99	2.37
	1.00	1.1	26.5	21.2	4.0	PC	3.093	72.961	1.82	>4	>4
3E	0.50	1.1	26.5	12.3	5.0	PC	0.373	5.497	0.92	1.94	2.18
	0.46	1.1	30.5	12.3	5.0	PC	0.376	5.472	0.92	1.93	2.15
3B	1.00	1.1	26.5	21.2	5.0	PC	3.245	63.90	1.82	>5	>5
	1.20	0.6	26.5	21.2	5.0	PC	2.875	57.955	1.73	>5	>5
	0.92	1.1	30.5	21.2	5.0	PC	3.250	63.379	1.85	>5	>5
	1.12	1.1	21.5	21.2	5.0	PC	2.695	47.791	1.74	>5	>5
	0.676	2.5†	26.5	21.2	5.0	PC	2.291	38.465	1.92	4.26	>5
3D	0.50	1.1	26.5	12.3	9.0	PC	0.373	5.111	0.92	1.88	2.04
3A	1.00	1.1	26.5	21.2	9.0	PC	3.149	46.01	1.84	3.95	4.47

*Thickness of conductive lid overlying convecting ice.

†Asteroid impact using serpentine equation of state (37).

REPORTS

We simulated impacts that would produce transient craters with diameters between ~ 12 and ~ 21 km. These are lower limits for the transient crater diameters predicted for Europa's largest central peak crater (Pwyll) and the multiple-ring craters, respectively (23). These limits were chosen to provide a lower bound for the ice thickness. However, due to uncertainties in crater scaling, the transient craters could have been up to 30% larger (28). Using Pi-group scaling (33, 34) and the parameters discussed, we calculated projectile diameters of ~ 0.5 and ~ 1.0 km for the 12- and 21-km-diameter transient craters, respectively. To investigate the effects of projectile velocity and porosity on melt and vapor production, in some cases we scaled the projectile size to maintain constant transient crater size (Table 1).

For the target, we used two scenarios: (i) an ice layer 4, 5, or 9 km thick with a purely

conductive, pre-impact temperature gradient between $T_{\text{surf}} = 110$ K (4) and $T_{\text{base}} = 270$ K over liquid water and (ii) a 3-km-thick conductive lid (a minimum value chosen to provide a limiting case) over warm, convecting ice (15, 16). In the latter scenario, we used a linear, pre-impact temperature gradient between $T_{\text{surf}} = 110$ K and $T_{\text{base}} = 255$ K for the conductive lid and a pre-impact temperature of 255 K for the convecting ice.

Unlike impacts into terrestrial targets, we found that for a constant transient crater diameter, the depths of the melt and vapor regions produced in the European simulations were relatively insensitive to variations in projectile velocity and porosity (even an asteroidal composition made little difference). This is because the shock pressures at which ice melts and vaporizes are below the level at which velocity and po-

rosity variations have significant effects (Fig. 4).

The larger projectile vaporizes the target ice to a depth of ~ 2 km in all cases modeled (Fig. 3, A through C). The 9-km-thick crust is completely melted to a depth of ~ 4 km (Fig. 3A); however, the complete melt region penetrates to the bases of the 4- and 5-km-thick crusts and the 3-km-thick conductive lid (Fig. 3, B and C). Complete melt-through to liquid water or warm, low-viscosity ice during crater formation is not inconsistent with the shallow, disrupted central regions and the lack of central peaks or peak rings in Europa's two multiple-ring structures [Web fig. 1 (24)]. However, central peak formation and preservation depends on the rheology of the surrounding material, which CSQ cannot model. Consequently, these simulations cannot provide an upper limit on ice thickness.

The smaller projectile vaporizes purely conductive ice to a depth of ~ 1 km, completely melts it to a depth of ~ 2 km, and partially (50%) melts it to depths of up to 2.4 km (e.g., Fig. 3, D and E). For the simulation with a 3-km-thick conductive lid over convecting ice (Fig. 3F), the depths of the complete vaporization and melting regions are within $\sim 10\%$ of those in the purely conductive simulations (Fig. 3, D and E). However, the region in which 50% melting occurs is considerably larger, extending to a depth of 4.4 km, well into the convecting ice (Fig. 3F). Under a central peak 5 km across and 500 m high [comparable to Pwyll's (25) (Fig. 2F)], the effective viscosity of ice at 255K would be $\sim 10^{13}$ Pa s (35), which yields a relaxation time of < 1 year. In this short time, ice ≥ 20 m below the surface cools < 10 K, so the existence of Pwyll's central peak precludes pen-

Fig. 1. Map of crater locations on Europa. Solid circles represent craters without central peaks. Open circles with inner solid circles represent central peak craters. Circles around plus signs represent craters not imaged at high enough resolution to unambiguously discern central peaks. Asterisks represent the two unusual impact structures, Taliesin and Tegid. Three nested rings represent multiple-ring structures. The maximum extent of each symbol is proportional to the diameter of the crater it represents. (Some empty regions are due to gaps in the high-resolution coverage.)

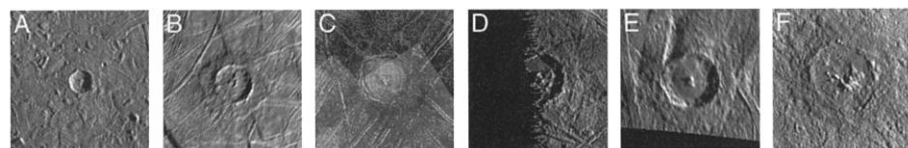
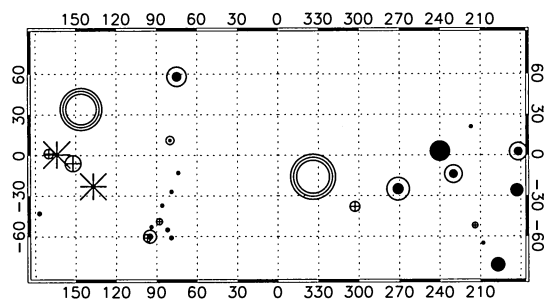


Fig. 2. Galileo images of European central peak craters. (A) Brigid (11°N , 80°W), $D = 8.5$ km. (B) Grainne (60°S , 95°W), $D = 13.5$ km. (C) Cilix (2.6°N , 182°W), $D = 18.4$ km. (D) Amergin (14°S , 230°W), $D = 18.6$ km. (E) Maeve (58°N , 75°W), $D = 20.4$ km. (F) Pwyll (25°S , 271°W), $D = 23.7$ km. All images are at a resolution of 250 m/pixel and each is illuminated from the right except Cilix (C), which was observed at high sun.

Fig. 3. Model results for impacts of large (A through C) and small projectiles (D through F) into 9-km-thick ice (gray) over liquid water (A) and (D), 5-km-thick ice (gray) over liquid water (black) (B) and (E), and 3-km-thick conductive lid (light gray) over convecting ice (dark gray) (C) and (F). Solid, dotted, and dashed lines show the regions of complete vaporization, complete melting, and 50% melting, respectively.

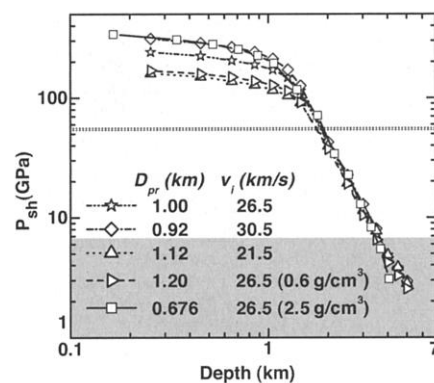
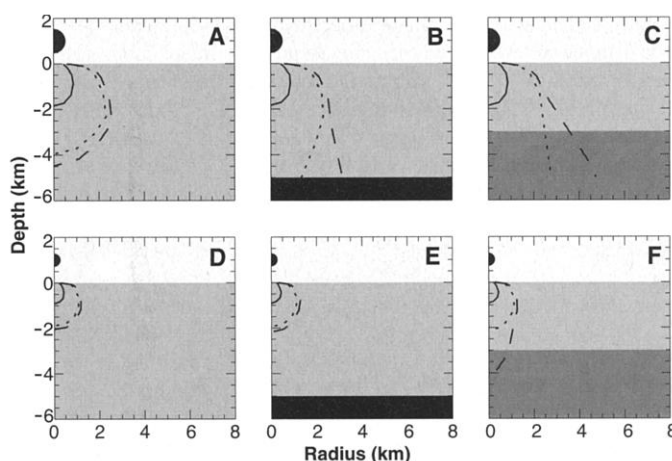


Fig. 4. Peak shock pressure versus depth for simulations of a 21.2-km-diameter transient crater. Projectile density is 1.1 g/cm³, unless otherwise noted. The 2.5-g/cm³ density is an asteroid. Light gray shading indicates shock pressures at which complete melting of ice occurs ($1 < P < 6.7$ GPa) at temperatures appropriate for this study (110 to 270 K). Horizontal dotted lines delimit the range of shock pressures at which complete vaporization occurs ($54 < P < 56$ GPa). For comparison, silicate rocks typically melt at ~ 50 to 60 GPa.

etration into a layer of warm ice. Furthermore, the 50% melt contour would completely penetrate a 3-km-thick layer of ice overlying liquid water at 270 K. Complete melt-through of a European ice shell during cratering would preclude central peak formation. The crater Mannán [Web fig. 2 (24)], which is comparable in diameter to Pwyll (Fig. 2F), does not have a well-defined central peak (23). This could be the result of an impact into thinner or warmer ice that hindered formation or preservation of a central peak, suggesting that local variations in temperature gradient or ice thickness may exist.

Because several, widely distributed European craters exhibit central peaks, our simulations demonstrate that at the times and locations these craters formed, a cold ice layer could not have been as thin as 3 to 4 km. Although complete melt-through of the ice layer does not occur in the simulations with slightly thicker ice, our transient crater sizes are lower limits. Moreover, impacts disrupt target material well beyond the zone of partial melting (36), so our simulations put a lower limit on the thickness of the ice. Therefore, we conclude that an ice shell must have been more than 3 to 4 km thick at the times and locations of complex crater formation.

References and Notes

1. P. M. Cassen, S. J. Peale, R. T. Reynolds, in *Satellites of Jupiter*, D. Morrison, Ed. (Univ. of Arizona Press, Tucson, AZ, 1982), pp. 93–128.
2. S. W. Squyres, R. T. Reynolds, P. M. Cassen, S. J. Peale, *Nature* **301**, 225 (1983).
3. M. N. Ross, G. Schubert, *Nature* **325**, 133 (1987).
4. G. W. Ojakangas, D. J. Stevenson, *Icarus* **81**, 220 (1989).
5. P. Helfenstein, E. M. Parmentier, *Icarus* **61**, 175 (1985).
6. A. S. McEwen, *Nature* **321**, 49 (1986).
7. P. E. Geissler *et al.*, *Nature* **391**, 368 (1998).
8. G. V. Hoppa *et al.*, *Icarus* **137**, 341 (1999).
9. P. M. Schenk, W. B. McKinnon, *Icarus* **79**, 75 (1989).
10. M. H. Carr *et al.*, *Nature* **391**, 363 (1998).
11. G. V. Hoppa, B. R. Tufts, R. Greenberg, P. E. Geissler, *Science* **285**, 1899 (1999).
12. M. G. Kivelson *et al.*, *Science* **289**, 1340 (2000).
13. C. Zimmer, K. K. Khurana, M. G. Kivelson, *Icarus* **147**, 329 (2000).
14. J. D. Anderson *et al.*, *Science* **281**, 2019 (1998).
15. R. T. Pappalardo *et al.*, *Nature* **391**, 365 (1998).
16. W. B. McKinnon, *Geophys. Res. Lett.* **26**, 951 (1999).
17. R. Greenberg, P. Geissler, B. R. Tufts, G. V. Hoppa, *J. Geophys. Res.* **105**, 17551 (2000).
18. P. E. Geissler, D. P. O'Brien, R. Greenberg, *Lunar Planet. Sci. Conf. XXXII*, 2068 (2001).
19. D. P. O'Brien, P. Geissler, R. Greenberg, *Icarus*, in press.
20. J. A. Rathbun, G. J. Musser Jr., S. W. Squyres, *Geophys. Res. Lett.* **25**, 4157 (1998).
21. R. T. Pappalardo *et al.*, *J. Geophys. Res.* **104**, 24015 (1999).
22. L. M. Prockter, R. T. Pappalardo, *Science* **289**, 941 (2000).
23. J. M. Moore *et al.*, *Icarus* **151**, 93 (2001).
24. Web figures 1 and 2, Web table 1, and text are available at Science Online at www.sciencemag.org/cgi/content/full/294/5545/1326/DC1.
25. J. M. Moore *et al.*, *Icarus* **135**, 127 (1998).
26. R. A. F. Grieve, P. B. Robertson, M. R. Dence, *Proc. Lunar Planet. Sci. Conf.* **12A**, 37 (1981).
27. C. M. Pieters, *Science* **215**, 59 (1982).
28. H. J. Melosh, *Impact Cratering: A Geologic Process* (Oxford, New York, 1989).
29. S. L. Thompson, *Tec. Rep. SAND77-1339*, (Sandia National Laboratories, Albuquerque, NM, 1979).
30. S. L. Thompson, H. S. Lauson, *Tec. Rep. SAND89-2951* (Sandia National Laboratories, Albuquerque, NM, 1972).
31. K. Zahnle *et al.*, *Icarus* **136**, 202 (1998).
32. E. Asphaug, W. Benz, *Icarus* **121**, 225 (1996).
33. R. M. Schmidt, K. R. Housen, *Int. J. Impact Eng.* **5**, 543 (1987).
34. Scaling calculations performed using code developed by H. J. Melosh, available at www.lpl.arizona.edu/tekton/crater.html.
35. W. B. Durham, S. H. Kirby, L. A. Stern, *J. Geophys. Res.* **102**, 16293 (1997).
36. H. J. Melosh, *J. Geophys. Res.* **87**, 371 (1982).
37. L. Brookshaw, Working Paper Series SC-MC-9813 (Univ. of Southern Queensland, Queensland, Australia, 1998); available at www.sci.usq.edu.au/cgi-bin/wp/research/workingpapers#1998.
38. Supported by NASA grants NAG5-8937 and NAG-9112. We are indebted to H. J. Melosh, R. D. Lorenz, A. S. McEwen, and L. P. Keszthelyi for helpful discussions and for reviewing the manuscript. We are also grateful to two anonymous reviewers who provided helpful comments.

14 May 2001; accepted 2 October 2001

Centennial-Scale Holocene Climate Variability Revealed by a High-Resolution Speleothem $\delta^{18}\text{O}$ Record from SW Ireland

Frank McDermott,¹ David P. Mattey,² Chris Hawkesworth³

Evaluating the significance of Holocene submillennial $\delta^{18}\text{O}$ variability in the Greenland ice cores is crucial for understanding how natural climate oscillations may modulate future anthropogenic warming. A high-resolution oxygen isotope record from a speleothem in southwestern Ireland provides evidence for centennial-scale $\delta^{18}\text{O}$ variations that correlate with subtle $\delta^{18}\text{O}$ changes in the Greenland ice cores, indicating regionally coherent variability in the early Holocene. Evidence for previously undetected early Holocene cooling events is presented, but mid- to late-Holocene ice rafting in the North Atlantic appears to have had little impact on $\delta^{18}\text{O}$ at this ocean margin site.

It is widely accepted that climate variability on time scales of 10^3 to 10^5 years is driven primarily by orbital, or so-called Milankovitch, forcing. Less well understood is the cause of the centennial- to millennial-scale variability that characterizes the $\delta^{18}\text{O}$ records of both the glacial and interglacial intervals of the GRIP and GISP2 ice cores (1, 2), yet this higher frequency variability may be important for predicting future climate change. Unlike the last interglacial (isotope stage 5), the Holocene [the last 11,700 years or 11.7 thousand years before the present (ky B.P.)] appeared to be anomalously stable because $\delta^{18}\text{O}$ in the GRIP and GISP2 ice cores seemed to be relatively constant (1, 2). More recently, millennial-scale climate variability has been detected in several Holocene climate proxy records, but there is little consensus about the precise timing, amplitude, or cause of these fluctuations (3–10). An emerging paradigm is that sub-Milankovitch climate variability is driven by a weak internal quasi-periodic (1500 ± 500 year) forcing of unknown origin that operates irrespective of whether the system is in a glacial or an interglacial mode (5, 9, 10). In the context of concerns about the impact of anthro-

pogenic greenhouse gases, it is important to establish whether these relatively low-frequency (~1500 year) events or higher frequency oscillations might determine the natural trends in global mean temperatures over the next few centuries. Therefore, a key question is the extent to which subtle higher frequency (century-scale) $\delta^{18}\text{O}$ variations in the Holocene sections of the Greenland ice cores reflect regional climatic signals rather than local effects or noise. Until now, that has been difficult to test, due to a paucity of sufficiently high resolution palaeoclimatic records. But here we present a newly found high-resolution O isotope time series for a well-dated stalagmite (CC3) from Crag cave in southwestern Ireland (Fig. 1), which shows that these subtle features are regional and not local signals.

Approximately 1640 laser ablation $\delta^{18}\text{O}$ measurements (11) were carried out along the growth axis of the 465-mm-long stalagmite, resulting in a high-resolution Holocene $\delta^{18}\text{O}$ record (12–14). Chronological control is provided by 13 TIMS U-series dates [Web table 1 (13)]. Before 5 ky B.P., the resolution is 2 to 20 times better than that of the published (2-m segment) $\delta^{18}\text{O}$ data for the GRIP and GISP2 ice cores and is about a factor of two worse than that of the ice cores since 5.3 ky B.P. The average resolution is approximately an order of magnitude better than in the North Atlantic cores that record evidence for quasi-periodic

¹Department of Geology, University College Dublin, Dublin 4, Ireland. ²Geology Department, Royal Holloway College, University of London, Egham, Surrey, TW20 0EX, UK. ³Department of Earth Sciences, Bristol University, Bristol BS8 1RJ, UK.